JOURNAL OF Materials CHEMISTRY

The thio-sol–gel synthesis of titanium disulfide and niobium disulfide

Part 2.†—Morphology, defect structure and electrochemical characteristics of titanium disulfide

Mandyam A. Sriram and Prashant N. Kumta*

Department of Materials Science and Engineering, Carnegie Mellon University, Pittsburgh PA 15213, USA

Received 3rd April 1998, Accepted 3rd August 1998

The thio-sol–gel process has been used to synthesize TiS_2 powders exhibiting different morphologies, from randomly agglomerated to radially oriented TiS_2 crystallites from a single precursor. It has been shown that different heat-treatment conditions can be utilized to simultaneously control the morphology of the sulfide powder and its defect concentration. Thus a variety of morphologies with crystallite sizes in the range of 2 μm to less than 0.5 μm and with defect concentrations (x in $Ti_{1+x}S_2$) in the range of $0.003 \leqslant x \leqslant 0.03$ have been synthesized. The crystallite sizes have been quantified using scanning electron microscopy and defect concentrations have been measured by determining the lattice parameter of the crystal. The performance of these materials as cathodes in secondary lithium batteries has also been evaluated and correlated to the crystallite size distributions and defect concentration.

1 Introduction

In the thio-sol–gel process, metal alkoxides are reacted with sulfidizing agents in solution to form alkoxysulfide precipitates. These alkoxysulfide precipitates can be converted to the sulfide upon heat-treatment in H_2S. In the first part of this two-part series, the reaction mechanisms involved in the formation of the precursor, the precursor chemistry, and the influence of the solvent in the formation of the alkoxysulfide precipitates were reported using TiS_2 as the model system. Four different variations of the process were reported in the first part while the reaction mechanisms were studied in detail for the first two variations. In each case, the alkoxysulfide precipitates formed have different molecular structures and correspondingly convert to TiS_2 upon heat treatment in H_2S exhibiting significant variations in the temperature of formation and morphology. The details of the thio-sol–gel process and three other variations of the process have been described and discussed in detail in Part 1 of this series. Its application for the synthesis of niobium disulfide has also been described in Part 1. In this second part, we shall present a detailed study of the sulfide powders derived by the two most important variations of the thio-sol–gel process. In particular, the influence of heat-treatment conditions on the evolving morphology and the defect concentration have been carefully studied. The influence of these conditions on the crystallite size distribution and defect concentration have been quantified and their combined effect on the electrochemical properties of the powder has been presented.

2 Experimental procedure

In Part 1, four reactions were reported in order to illustrate the mechanism of the thio-sol–gel process. In order to further elucidate the effects of structure and morphology of the powder on its electrochemical properties, in this paper, we shall present a study conducted on the first two reactions (labeled reactions A and B). *Reaction A*: the reaction of titanium isopropoxide with H_2S conducted in anhydrous benzene. The same reaction conducted in anhydrous acetonitrile will be termed reaction A in acetonitrile. *Reaction B*: the reaction of titanium isopropoxide modified with benzenesulfonic acid (BSA) using a modification ratio $n=0.1$ (n is the molar ratio of BSA to Ti isopropoxide), conducted in anhydrous benzene.

We have chosen to study the powders obtained from these two reactions since they displayed the most significant variations in morphology. In addition to this, TiS_2 has also been synthesized by a conventional reaction between Ti metal and S. These powders will form the baseline material for comparing the properties of the chemically derived sulfide. The details of all the experimental procedures pertaining to the synthesis of TiS_2 following reactions A and B were reported in Part 1.

2.1 Comparison of structure and morphology of TiS_2 obtained using various reactions and heat-treatment conditions

Based on the results obtained from the experiments described in Part 1, various morphologies of single phase TiS_2 powders with different stoichiometries were obtained by controlled heat treatment conditions. The morphology was observed using an SEM (CamScan, Series 4) and the stoichiometry of the sulfides was determined by precise measurements of the lattice parameter. Samples for SEM observations were prepared by ultrasonicating the powders in hexane and dropping the suspension on a graphite stub. A high angle diffraction pattern was collected from $2\theta=90^\circ$ to 158° using Si powder as an internal standard (using a Rigaku θ/θ difractometer equipped with a diffracted beam monochromator). Between 10 and 15 peaks could be identified and measured precisely for each of the powders. Lattice parameters were determined using a least squares fitting algorithm. The defect concentrations were deduced from the c-axis lattice parameter.[1] The chemical synthesis procedure and heat treatment conditions of the powders selected for comparison are shown in Table 1. The heat treatments were designed based on results obtained from the above experiments (on reactions A and B) and thermodynamic calculations of defect concentrations outlined in the Appendix.

2.2 Characterization of TiS_2 as a cathode in batteries

The ability of TiS_2 to spontaneously intercalate Li atoms reversibly in the structure has been used to apply the material as a cathode in rechargeable battery systems. Whittingham[2] first measured the open circuit voltage (OCV) of a rechargeable

†Part 1, preceding paper.

Table 1 TiS_2 powders used to compare the defect structure and morphology

	Reaction	Solvent	Heat treatment in H_2S[a]	
1	A	Benzene	Fast	Slow
2	B	Benzene	Fast	Slow
3	A	Acetonitrile	—	Slow
4	Solid state synthesis[b]			

[a]Fast: 900 °C h^{-1} to 800 °C, dwell for 6 h, furnace cool to room temp. Slow: 60 °C h^{-1} to 800 °C, dwell for 6 h, cool at 120 °C h^{-1} to room temp. [b]Stoichiometric amounts of Ti powder and S powder were sealed in an evacuated ampoule. Ti was placed at the bottom with S on top and the ampoule was heated in an upright position. The heating schedule was as follows: 30 °C h^{-1} to 200 °C, dwell for 3 h, 30 °C h^{-1} to 500 °C, dwell for 36 h, 60 °C h^{-1} to 600 °C, dwell for 3 h, 100 °C h^{-1} to 500 °C, dwell for 1 h and furnace cooled to room temperature approximately at the rate of 60 °C h^{-1}. This heat treatment schedule was necessary to prevent a runaway reaction that could cause an explosion of the ampoule. After this heat treatment, a cake of TiS_2 was formed at the bottom of the ampoule, which was crushed, placed in a graphite boat and heated in flowing H_2S at 500 °C for 6 h.

{Li|$LiPF_6$ in propylene carbonate|TiS_2} battery. The sloping discharge results from the fact that there is only one phase in contact with the electrolyte, and the chemical potential of Li in this phase changes with composition. The intercalation reaction of Li in Li_yTiS_2 is highly reversible in the range $0 \leqslant y \leqslant 1$ and the life of the battery in this range is limited by other factors such as dendrite formation at the Li anode (if Li is used as the anode) or decomposition of the electrolyte. The theoretical specific capacity of TiS_2 for a discharge up to $LiTiS_2$ is 239 mA h g^{-1} and its specific energy is about 540 mW h g^{-1}. Cathode utilization (measured specific capacity divided by the theoretical specific capacity) can be measured by galvanostatic cycling in a three-electrode system using voltage cut-off limits measured between the cathode and a reference electrode. TiS_2 has an open circuit voltage of 2.5 V *vs.* Li and $LiTiS_2$ has a voltage of about 1.8 V also against Li. In our testing procedure test batteries were cycled between 2.5 and 1.7 V (reference *vs.* cathode). Since the voltage drops rather rapidly between 1.8 and 1.7 V, the contribution to cathode utilization in this region is very small. Discharging it below 1.7 V would cause the formation of Li_2TiS_2 at the surface. Therefore 1.7 V can be considered as the lowest practical voltage limit allowable during discharge, without inducing any permanent structural damage that may affect the long term cyclability of the cell. The theoretical specific capacity (Q_o) in this voltage range (2.5 to 1.7 V) has been assumed to correspond to $LiTiS_2$ (239 mA h g^{-1}).

Electrochemical performance of the powders synthesized by all the processes shown in Table 1 were evaluated by fabricating cathodes following the procedure described below. All handling of TiS_2 powders before and after preparation of the cathodes was accomplished in a glove box or a glove bag in the absence of air and moisture. A homogeneous slurry of the TiS_2 powder was prepared in trichloroethylene along with additions of acetylene black (5.19 wt.%), graphite (2.59 wt.%) and a copolymer binder (9.08 wt.%) (ethylene–propylene copolymer binder containing 60% ethylene fraction).The slurry was then coated onto an Al foil using a draw rod and dried at *ca.* 100 °C under vacuum for 12 h. Discs approximately 1 cm in diameter were punched out of the coated foil and weighed to estimate the weight of the active material. The cathodes were tested in prototype test cells, the details of which have been described elsewhere.[3]

The anode consisted of a piece of Li foil. The electrolyte used was 1 M $LiAsF_6$ in a mixture of 95% 2-methyltetrahydrofuran and 5% ethylene carbonate. Batteries were galvanostatically tested for 5 cycles using a discharge current density of 1 mA cm^{-2} and a charge current density of 2 mA cm^{-2}. End of discharge and charge were determined by cut-off voltages measured between the cathode and a lithium reference electrode. The battery was cycled between 2.5 and 1.7 V. After cycling, the cathode was recovered, cleaned and the Al foil weighed to estimate the weight of the active material more accurately. When the cathodes were weighed (before and after cycling) to a precision of ± 0.0001 g, this method offered a theoretical error in the measurement of efficiency (in percentage) of approximately $\pm 0.04\%$ absolute in the range of 70 to 90% efficiencies. However, deviations in the range of $\pm 0.5\%$ absolute were observed and could be attributed to inhomogeneities in the cathode coating. The efficiency values quoted are a result of an average of five cycles measured using two to three batteries (a total of 10 to 15 efficiency values).

3 Results and discussion

The mechanism involved in the thio-sol–gel process for the synthesis of TiS_2 has been described in detail in Part 1 of this series. Some of the important aspects from Part 1 are repeated below: (i) titanium alkoxides react with various sulfidizing agents to form alkoxysulfide precipitates; (ii) the alkoxysulfide precipitates convert to TiS_2 upon heat treatment in H_2S gas at temperatures above *ca.* 700 °C by releasing water and hydrocarbons; (iii) the morphology of the TiS_2 formed depends on the particular reaction used. In the four reactions that were studied, significant variations in morphology were observed, particularly between reactions A and B (reaction of plain titanium isopropoxide with H_2S and reaction of modified isopropoxide with H_2S respectively). These two morphologies are compared and discussed in the following section.

3.1 Comparison of the morphology of TiS_2 prepared from reactions A and B

The most noteworthy difference between the sulfides prepared by reactions A and B is the morphology of the powders. The formation of such varied microstructures can be related to differences (in molecular structure) between the precursors and their consequent reactions with H_2S, as well as anisotropy in the surface and bulk properties of TiS_2 crystals. The role of water formed as a byproduct of the gas–solid reaction may also need to be considered with regards to the evolution of morphology during the transformation of the precursor to the sulfide.

The hypothesis behind the role of water arises from similarities in the morphologies of the synthesized powders and the microstructure of TiS_2 thin films obtained using various deposition techniques (for example Kanehori *et al.*[4]). Although the morphological studies of this material have not been performed in detail, analogies can be drawn from studies conducted on MoS_2 thin films (which have an anisotropic structure similar to TiS_2) prepared by radio frequency sputtering.[5,6] In effect, it has been shown that the introduction of water during the formation of the films strongly influences the morphology. However, its role in influencing the deposition mechanisms on the surface of the substrate is unclear.

The possibility of the presence of water playing a role in the morphology of the synthesized powders in addition to the molecular structure and the anisotropic nature of TiS_2 cannot be ruled out in this case because water is inevitably formed due to the reaction between TiO_2 (which forms in the early stage of the conversion of the precursor to the sulfide) and H_2S. Thus, any effect that water might have on the nucleation and growth of TiS_2 is coupled with the molecular structure of the precursor. In addition to this, the effect of water must be gauged in terms of its instantaneous concentration, which implies that the kinetics of the reaction of H_2S with the amorphous precursor particles (which is again affected by molecular structure) is crucial.

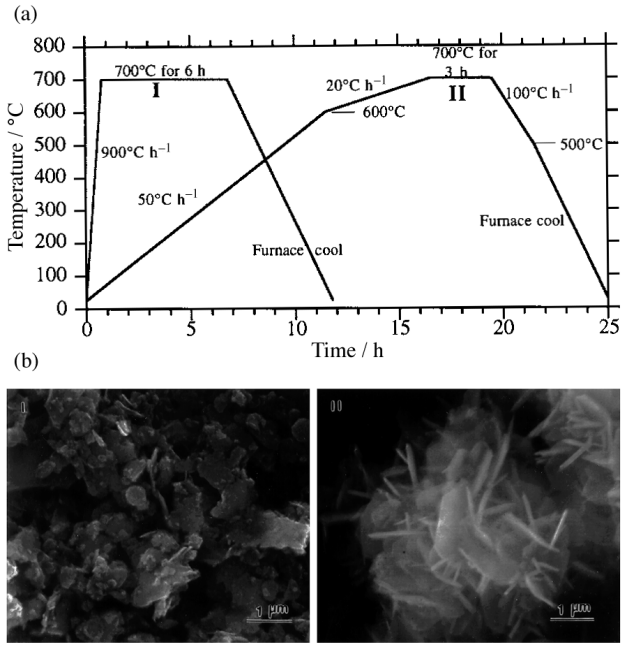

Fig. 1 (a) The temperature programs used for the heat treatments of the powder obtained from reaction A. (b) The corresponding morphologies of the two powders.

To illustrate this, an experiment was conducted to observe the variation in the morphology of the powders obtained from reaction A as a function of the heat treatment rate. The powders were subjected to two heat treatments as shown in Fig. 1(a). The heat treatments labeled I and II were conducted using approximately the same flow rates of H_2S. The corresponding morphologies that were observed are shown in Fig. 1(b), also labeled as I and II. The morphology in II distinctly resembles the product obtained by heat treating the precipitate obtained from reaction B at 700 °C, using a heating rate of 900 °C h^{-1} [see Fig. 7(c) in Part 1 of this series]. This clearly shows the influence of heat treatment parameters on the morphology. One of the most striking differences between the reactions occurring under these conditions is the kinetics of formation of TiS_2. The instantaneous concentration of water vapor is expected to be lower in II as compared to I due to the slower kinetics. In addition to this, the precipitate obtained from the second reaction is expected to be less susceptible to hydrolysis due to steric hindrance from the benzenesulfonyl groups attached to titanium. Hence the powders from the second reaction (heat treated at 900 °C h^{-1} to 700 °C for 6 h under flowing H_2S) could exhibit a morphology similar to the powder obtained from heat treatment schedule II performed on the precipitate of the first reaction.

Alternatively, another model could be envisaged which exploits the anisometric growth characteristics of TiS_2 and differences in nucleation rates per unit surface area of the precursor. The equilibrium shape of the TiS_2 crystal is a flat hexagonal prism, whose axis is parallel to the *c*-axis of the unit cell. The growth of the prism along the *c*-axis is much slower than perpendicular to it, which results in the observed platelet-like appearance of the material. The growth of TiS_2 occurs at the precursor–TiS_2 interface due to the reaction of the precursor with H_2S. Assuming that the initial nucleation causes the formation of TiS_2 crystals that are randomly oriented on the surface, at any angle of orientation where the growth is not radial, growth results in termination at a neighboring platelet. Therefore the only platelets that survive this competition are the ones that grow the fastest radially, namely the ones that have their *c*-axes oriented perpendicular to the radial direction. Based on this, the microstructures could be explained on the basis of different nucleation sites per surface area of the precursor. A uniformity on the surface at a finer scale could lead to the growth of platelets of similar sizes.

These results were utilized in designing further heat treatments to study the influence of defect structure and morphology of TiS_2 powders on their performance as cathodes in secondary lithium batteries. The results of these studies are presented and discussed in a later section of this paper.

3.2 Influence of heat treatment conditions on the morphology and defect structure of thio-sol–gel synthesized TiS_2

The defect structure and chemistry of TiS_2 both significantly influence the kinetics of intercalation of lithium which in turn affects the performance of the material as a cathode. In stoichiometric TiS_2, the site occupied by Ti (1a, with site symmetry $\bar{3}m$) can be chosen as the origin. Consequently, S resides on the 2d position (with site symmetry $3m$), with the coordinates (1/3, 2/3, z) and (2/3, 1/3, $-z$). In the case of stoichiometric TiS_2, $z=0.25$, which implies an ideal octahedral coordination of Ti by sulfur.[7] In $Ti_{1\pm x}S_2$ the excess Ti atoms reside on the 1b site (site symmetry $\bar{3}m$) at a displacement of (0, 0, 1/2) from the origin which is also the site for the intercalation of foreign atoms. The bonding between the S—S layers is increased by the presence of interstitial Ti atoms and this provides a barrier for intercalation by pinning together the S—S layers. Thompson *et al.*[1] have observed that in $Ti_{1.00}S_2$, ammonia intercalates in 2 h, while in $Ti_{1.1}S_2$ it requires 24 hours to achieve the same extent of intercalation. It was observed that the intercalation of larger molecules is even more sensitive to the stoichiometry. The intercalation of Li in TiS_2 is also similarly influenced. Kanehori *et al.*[8] have measured the diffusion coefficient of Li in TiS_2 and have shown the strong dependence of the kinetics of intercalation on the stoichiometry of the sulfide. The stoichiometry can be measured by chemical analysis or inferred from lattice parameter measurements. A careful study of the dependence of lattice parameter on stoichiometry has been conducted by Thompson *et al.*[1] which has been utilized in the current work to determine the stoichiometry of the material by the measurement of its *c*-axis lattice parameter. Lattice parameters of the crystalline sulfide powders prepared by the thio-sol–gel process have been measured to a precision of ± 0.001 Å and have been compared with TiS_2 synthesized by the conventional solid-state reaction.

The earliest work on the defect chemistry of TiS_2 was reported by Biltz and Ehrlich,[9] wherein they investigated (along with several synthesis methods) the influence of the partial pressure of sulfur [$p(S_2)$] on the Ti–S phase equilibria in the composition domain: 58.3 atom% to 79.6 atom% S. Winn and Steele[10] have performed a more detailed study and have measured the equilibrium $p(S_2)$ over $Ti_{1+x}S_2$ as a function of x and temperature. Their equilibrium data were reported with reference only to the S_2 component of the vapor and therefore can facilitate comparisons to be made based on this reference state. Their results show that there is a rapid increase in the equilibrium sulfur pressure as the stoichiometric composition is approached and that the sulfur vapor pressure in equilibrium with near stoichiometric TiS_2 is higher at higher temperatures. Finally, a thorough compilation of the defect chemistry of TiS_2 has been presented by Molenda *et al.*,[11] which brings into perspective all the data pertaining to the stoichiometry of TiS_2. The equilibrium data measured by Winn *et al.*[10] and compiled by Molenda *et al.*[11] have proved to be very useful in the current work. Since all of the heat treatment experiments in this work were conducted in an atmosphere of H_2S, the equilibrium stoichiometries have been calculated as a function of temperature in an H_2S atmosphere using the data compiled by Molenda *et al.*[11] and the equilibrium data available for the decomposition of H_2S. This calculation has been outlined in the Appendix.

Table 2 Summary of crystallite size measurements (in μm)[a]

	From number distribution		From mass distribution		Particle size range	
Process	Mean	Median	Mean	Median	Min.	Max.
Solid state reaction	1.9	1.6	3.8	Multimodal	0.5	9
Reaction A (fast)	0.4	0.4	0.6	0.6	0.1	1
Reaction B (fast)	1.3	1.3	1.7	*ca.* 2	0.7	2.6
Reaction A (slow)	—	Multimodal 0.1 and 0.6	0.3	Multimodal 0.1 and 0.6	0.3	0.9
Reaction B (slow)	1.3	1.2	1.7	1.6	0.5	2.6

[a]Values calculated from 100 to 200 measurements of basal plane dimensions.

From the results described in the previous section, it is clear that heat treatment conditions influence the morphology of the titanium sulfide powders. In addition, from the calculations shown in the Appendix, there is a good likelihood that the cooling rate during the heat treatment influences the stoichiometry (defect concentration) of the material—a material closer to stoichiometry could be obtained by decreasing the cooling rate. In order to study this, TiS_2 powders were synthesized using 'slow' and 'fast' heat treatment conditions as shown in Table 1. X-Ray peak width analysis involving the use of the Warren–Averbach method and Scherrer's approximation could not be applied in this case because of the wide

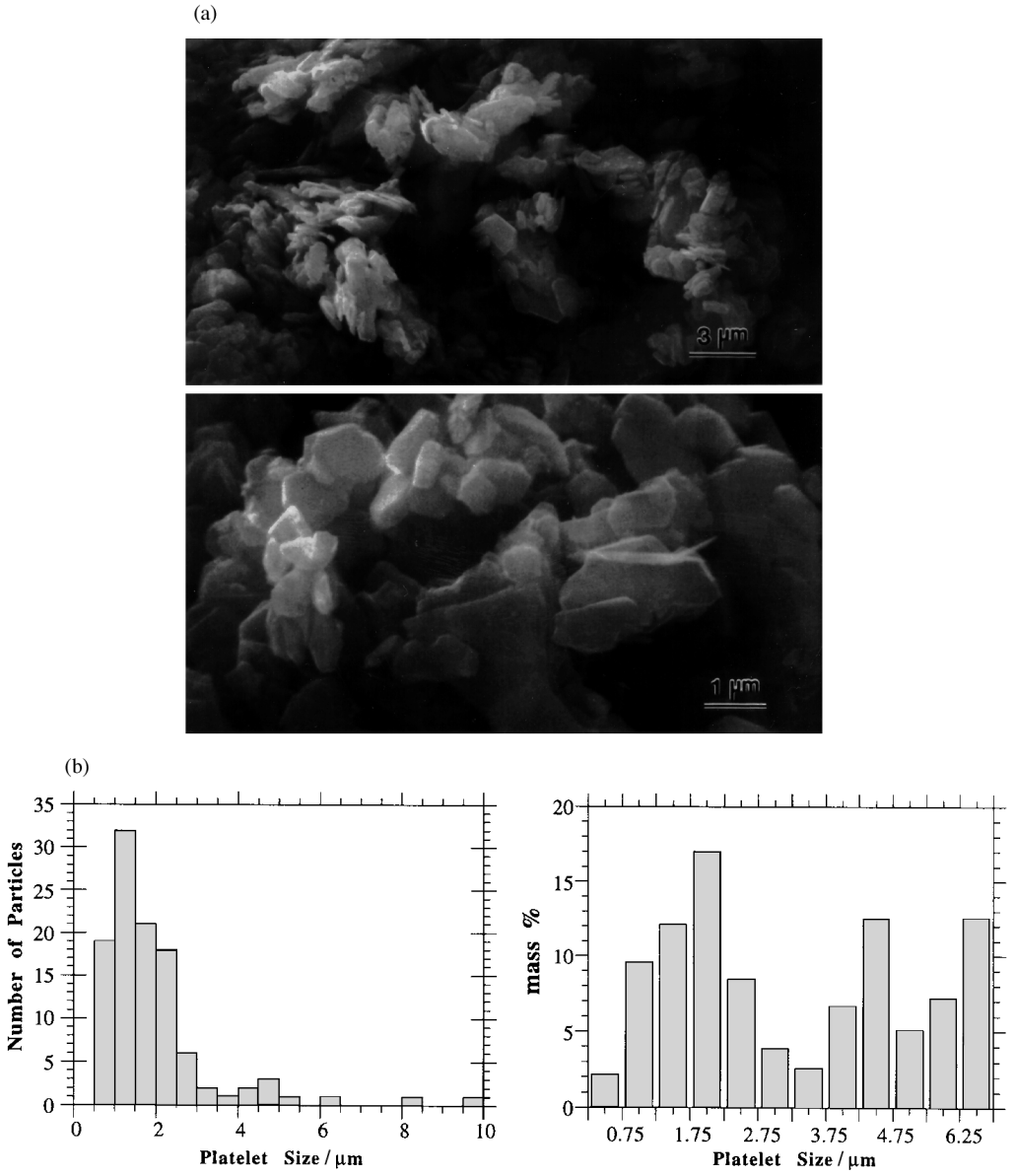

Fig. 2 (a) Morphology of powders obtained by the solid state reaction of elemental Ti and S in an evacuated quartz ampoule. (b) The number and mass distribution of platelets in the powder.

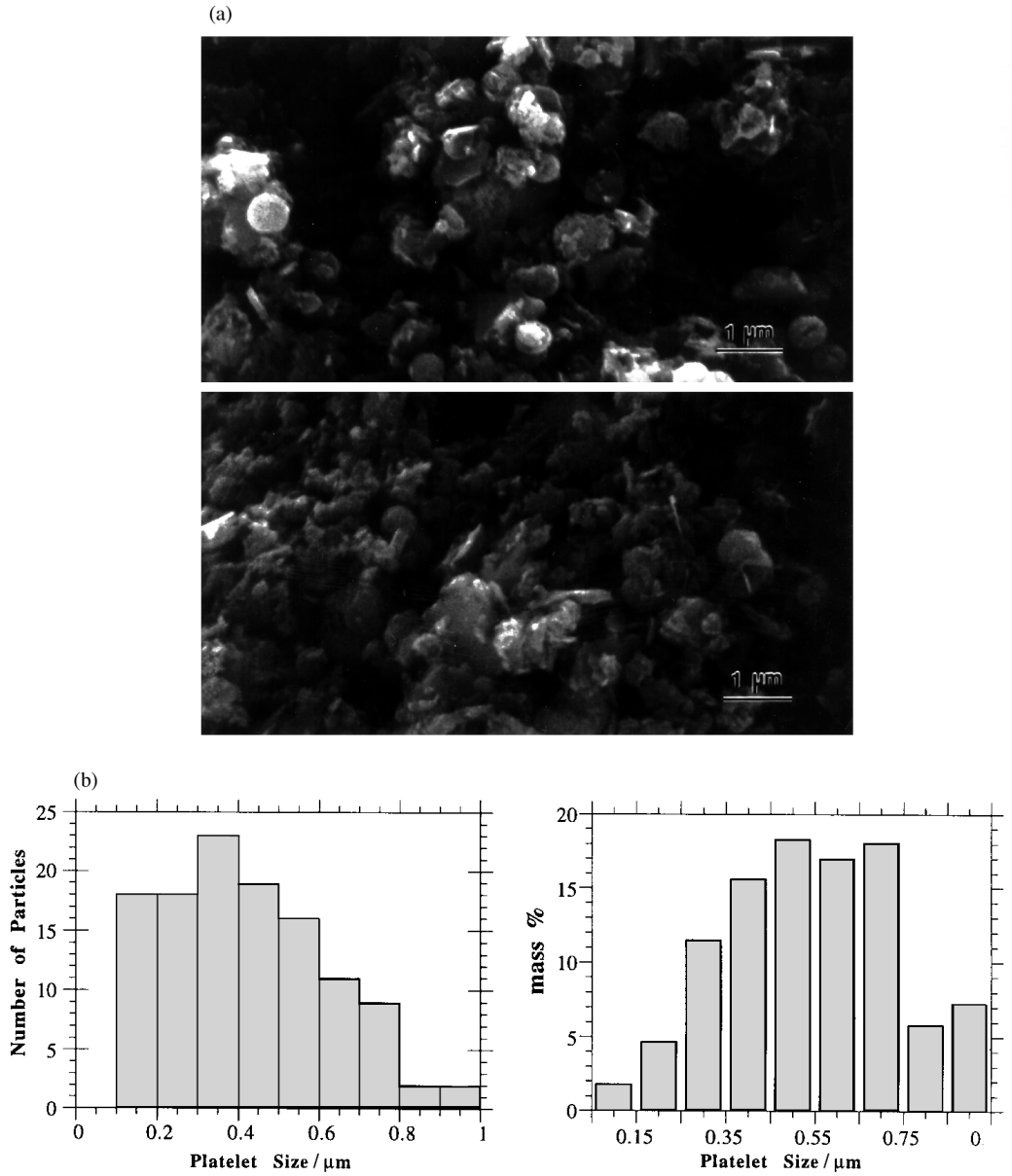

Fig. 3 (a) SEM micrograph of powders obtained by fast heat treatment of precipitate from reaction A conducted using benzene as a solvent. (b) The number and mass% platelet size distributions of the powder.

distribution of crystallite dimensions. Therefore particle sizes were measured from SEM photomicrographs taken from 2 to 3 different areas of the sample. A summary of the statistical data obtained from these measurements is shown in Table 2.

The SEM micrographs of TiS_2 powders are displayed in Fig. 2–6 along with approximate crystallite size distributions measured from at least three different areas of the sample at two different magnifications ($\approx 6000\times$ and $\approx 10000\times$). In all the micrographs seen, the variation in the prismatic plane dimension of the platelets was small compared to the variation in the basal plane dimension. The crystallite size distributions (of the basal plane dimension) are displayed as the number of particles per size interval as well as the mass percent of crystallites per size interval. The mass of crystallites of a particular size was calculated by assuming a sharp distribution of the thickness of the platelets, which yields the following relationship for the mass fraction:

$$m_i = \frac{M_i}{M} = n_i d_i^2 / \sum_i n_i d_i^2 \quad (1)$$

where n_i is the number of particles of size d_i and M_i is the total mass of all particles of size d_i. This approximate relationship describing the mass percent distributions is more appropriate for the current study because of the following reason.

If the coulombic efficiency of the material is related to the crystallite size we could obtain a relation for the capacity as well, and if we assume that m_i mass fractions of crystallites of size d_i are mixed together, and if crystallites of size d_i exhibit a specific capacity C_i, then the specific capacity of the mixture could be represented as

$$C = \sum_i m_i C_i \quad (2)$$

Therefore, the mass fraction distribution of crystallites of size d_i directly relates the specific capacity of the powder to the specific capacity of the crystallite. On the other hand, if the number fraction distribution of particles is considered, then the capacity of the mixture can be represented as

$$C = \sum_i f_i M_i C_i \quad (3)$$

where f_i is the number fraction of crystallites of size d_i and M_i

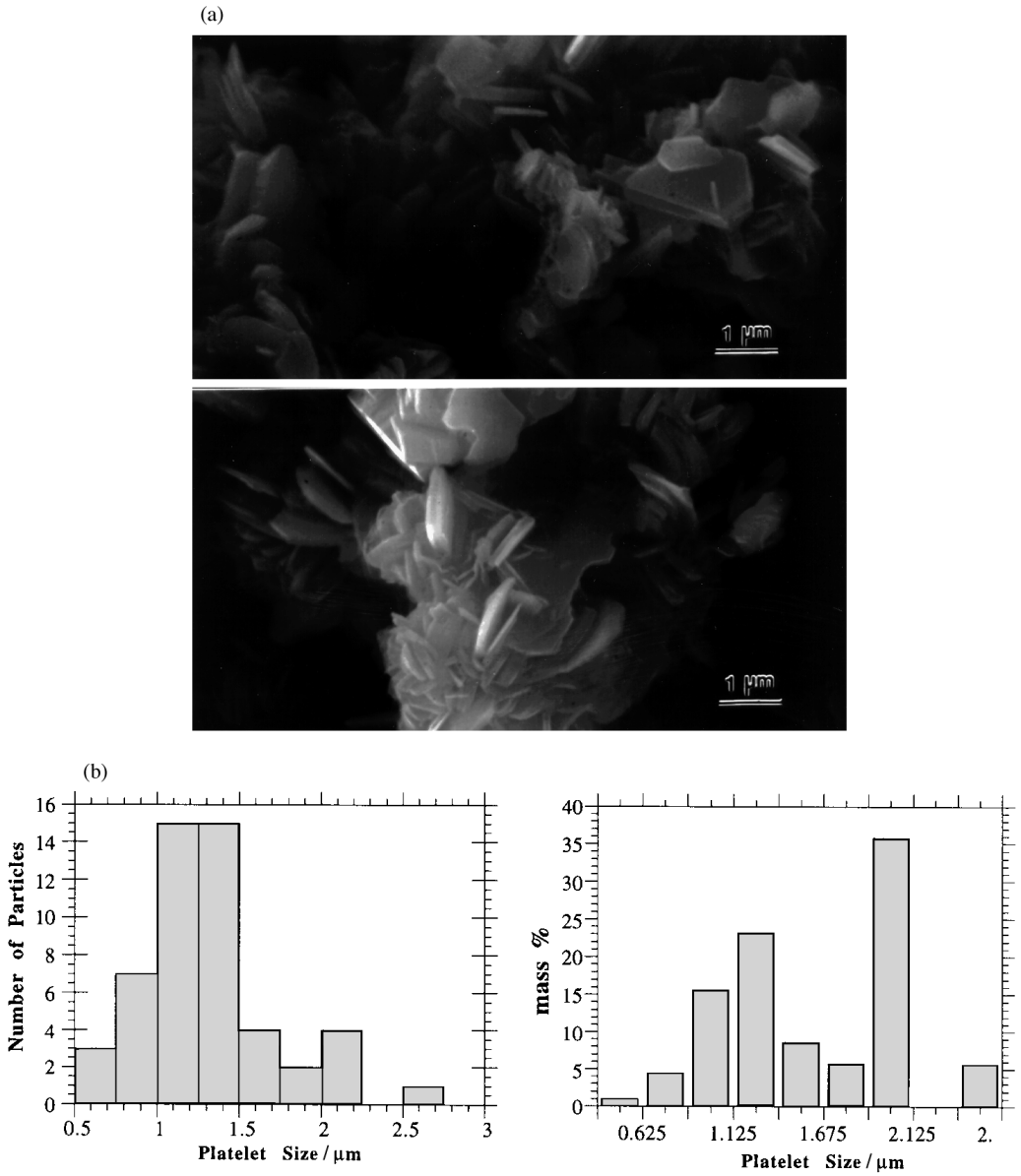

Fig. 4 (a) SEM micrograph of powders obtained by fast heat treatment of precipitates from reaction B using fast ramping and cooling rates. (b) Number and mass% platelet size distributions measured from SEM micrographs.

is the mass of the particle of size d_i. M_iC_i is the total charge that a crystallite of size d_i can acquire and it is not a specific quantity. Qualitatively this can be explained by the fact that the capacity of the powder is determined more by the mass fraction of the particles of a particular size rather than the number fraction since capacity is measured in terms of charge/mass.

The morphology of the powders obtained by the solid state reaction of elemental Ti and S is shown in Fig. 2(a) and the number and mass fraction distributions determined from the relations shown above are represented in Fig. 2(b). The micrographs clearly shows a wide platelet size distribution ranging from 0.5 to 9 μm. A mean value of 2 μm is obtained from the number distribution and a mean value of 3.8 μm is obtained from the mass% distribution. Such a microstructure comprising of randomly agglomerated platelets that vary in size is characteristic of the solid state process and is a result of the prolonged reaction conducted at 500 °C for 36 h. Another characteristic is the agglomeration of the fine platelets to form large clumps which range in size from 6 to 10 μm.

Fig. 3(a) shows micrographs of powders obtained from reaction A conducted in benzene heat treated to 800 °C using fast ramping and cooling rates. The powder consists of randomly agglomerated platelets varying in sizes from 0.1 to 1 μm. In addition, there are a few spherical particles which have retained their shape from the original as-prepared precursor stage. The mean crystallite sizes estimated from number distribution and from mass% distribution are 0.4 and 0.6 μm respectively. In comparison to the powder synthesized using the conventional reaction between the elements, the particle size distribution is narrow in this case [see Fig. 3(b)].

Fig. 4(a) shows the morphology of the powders obtained from reaction B (modified alkoxide) heat treated at 800 °C using fast heat treatment conditions. In this case the platelets are in the range of 0.7 to 2.6 μm in size and the distributions are shifted to larger sizes in comparison to the powders obtained from reaction A [Fig. 4(b)]. The mean crystallite sizes estimated from number distribution and mass% distribution are 1.3 and 1.7 μm respectively.

Fig. 5(a) shows the morphology of the powder derived from reaction A in benzene heat treated at 800 °C using slow ramping and cooling rates. A pseudomorphous transformation is apparent in some of the particles seen from the uniform growth of platelets (0.3 to 0.9 μm in size) in a radial direction

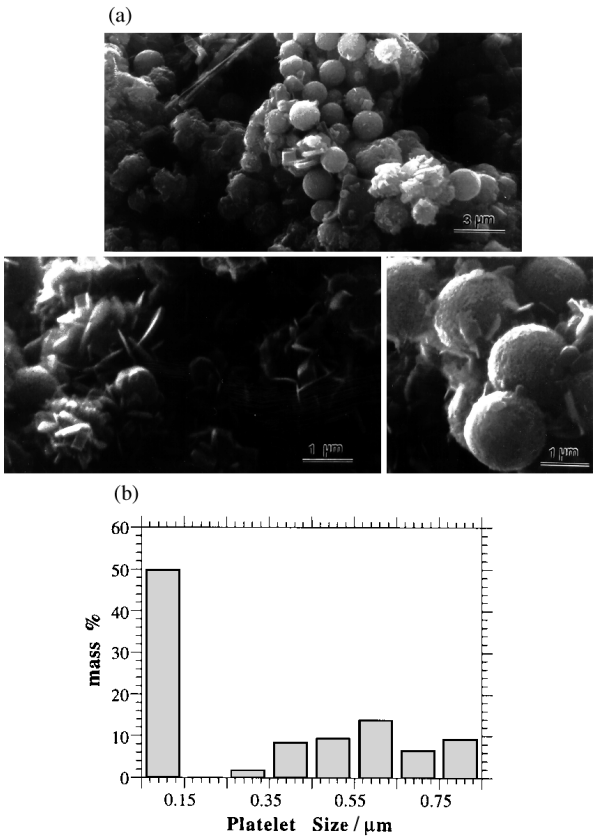

Fig. 5 (a) SEM micrographs of powders obtained from reaction A conducted in benzene heat treated using slow ramping and cooling rates. Approximately half of the precipitate particles retain their original spherical shape with platelets in the range of 0.1 μm. The rest of the particles have undergone a pseudomorphous transformation showing plates (≈0.6 μm) growing out of the original spherical particle. (b) The mass% size distribution of platelets. The first bar in the histogram has been estimated (see text for details).

out of the original spherical particle. In addition to this, the micrographs also reveal several spherical particles that have retained their original shape. As shown in the micrographs, these spherical particles show significant surface roughening at higher magnifications indicative of very fine (<0.1μm) crystallites of TiS_2. In this case it was possible to estimate from several SEM micrographs that approximately 50% of the particles retain their spherical shape. Therefore this powder approximately exhibits a bimodal distribution of crystallite sizes, centered around 0.1 μm and 0.6 μm as shown in Fig. 5(b). The mean from the number distribution could not be determined but the mean from the mass distribution was estimated to be 0.3 μm.

The micrographs of TiS_2 powders obtained by slow heat treatment of precipitates derived from reaction B in benzene are shown in Fig. 6(a). The morphology is similar to that observed using fast heat treatment conditions for the same precursor, showing crystallites varying in size from 0.5 to 2.6 μm. The number-average crystallite size is 1.3 μm and the mass-average is 1.7 μm [from Fig. 6(b)].

It is clear that the powders derived from the thio-sol–gel process exhibit finer crystallite sizes in comparison to the powder synthesized by a reaction between the elements (see Table 2). The powders obtained from reaction A show smaller average crystallite sizes in comparison to powders obtained from reaction B. In addition, powders obtained using slow heat treatment of precipitates obtained from reaction A yield smaller crystallites in comparison to fast heat treatments of the same precipitate. Powders derived from reaction B, however, show similar crystallite sizes under both heat treatment conditions.

In addition to these synthesis approaches, precipitates obtained from reaction A using acetonitrile as a solvent were also heat treated in H_2S using slow heat treatment conditions. SEM micrographs of the powder are shown in Fig. 7. The crystallite sizes of this powder are extremely small (≤0.5 μm). Only the large platelets (0.5 μm in width) can be clearly observed because of the limited resolution of the instrument. The boundaries of smaller platelets which exist as agglomerates and dispersed among larger platelets cannot be clearly distinguished. However, the micrographs do show qualitatively the fine nature of the crystallites.

The stoichiometry (x in $Ti_{1+x}S_2$) of all these powders was measured by the method described in the experimental procedure and is shown in Table 3. As expected from the calculation (shown in the Appendix), powders obtained using slow cooling rates during the heat treatment yield sulfides closer to stoichiometry in comparison to powders obtained using fast cooling rates. The lattice parameter of TiS_2 obtained by slow heat treatments of the precipitates from reaction A conducted in acetonitrile could not be measured with sufficient accuracy because of significant peak broadening observed at higher angles. However in all previous experiments, consistent values of x (in $Ti_{1+x}S_2$) have been obtained from different precursors using identical cooling rates. Therefore in this case too, the stoichiometry of the sulfide can be expected to be in the vicinity of $Ti_{1.003}S_2$.

3.3 Influence of crystallite size and defect concentration on electrochemical performance

The experimental procedure for measuring cathode utilization is described in section 2.2. The test batteries were charged and discharged over 5 cycles. During the test, a constant current is applied while the voltage between a lithium reference electrode and the cathode is measured. The raw data obtained from the test therefore consist of the variation of voltage with time for each cycle. During the intercalation of Li, there is one electron transferred for every Li atom that intercalates into the active material. Therefore, at a constant current, the time axis can be converted to composition of the intercalated material, *i.e.* x in Li_xTiS_2:

$$x = \frac{it}{Fm} \tag{4}$$

where i is the current, t is the time, F is Faraday's constant (96485 C mol^{-1}) and m is the number of moles of active material. During the rest cycle, there is no current flowing between the anode and the cathode and therefore the composition remains constant.

Typical charge discharge characteristics *versus* a composition axis are shown in Fig. 8. The first discharge step commences at $x=0$ since the starting material is TiS_2 corresponding to the charged state. The solid state synthesized material intercalates lithium to $Li_{0.9}TiS_2$, however, it can be deintercalated (during charging) to only $Li_{0.2}TiS_2$. On the other hand, the deintercalation of all the thio-sol–gel synthesized materials proceeds to *ca.* $Li_{0.1}TiS_2$. The utilization of the thio-sol–gel synthesized materials prepared using fast heat treatment rates is low, mainly because intercalation does not proceed to significant extents during discharging. On the other hand, all the slow heat treated powders show significant improvements over the other materials, exhibiting excellent intercalation as well as deintercalation of Li into the sulfide. The cathode utilization has been plotted for all the materials as a function of cycle number in Fig. 9. The thio-sol–gel derived powders synthesized using fast heat treatment conditions, as well as the solid state synthesized powders show utilization values below 80%. All the powders synthesized using slow heat treatments however, show very high utilizations (>85%). The best utiliz-

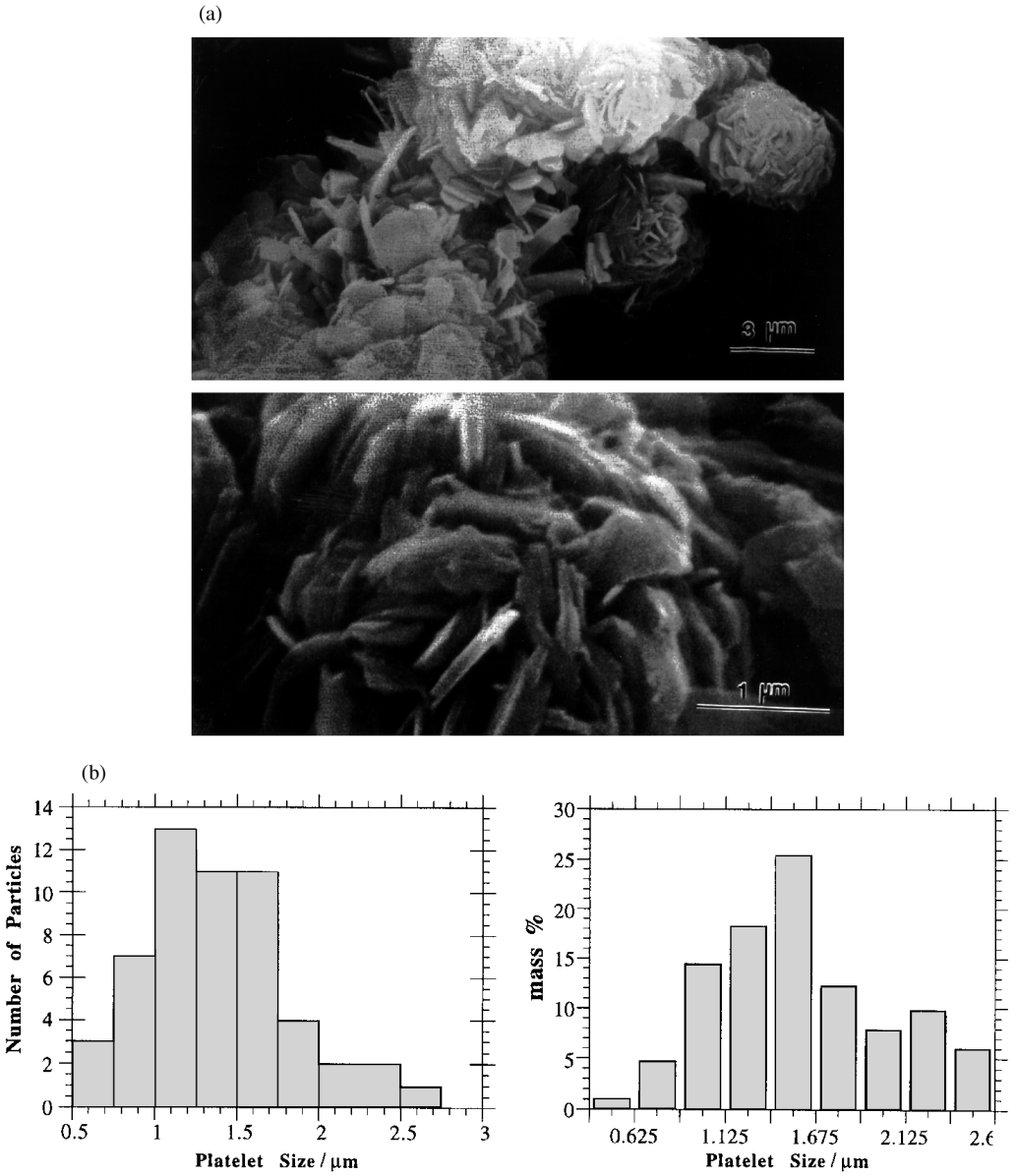

Fig. 6 (a) SEM micrograph of powders obtained from reaction B in benzene heat treated using slow ramping and cooling rates. (b) Number and mass fraction distributions of platelet size measured from SEM micrographs.

ation values (*ca.* 90%) are shown by the powders obtained from reaction A using acetonitrile as a solvent heat treated using slow ramping and cooling rates.

Table 4 shows a comparison of the cathode utilization of all the TiS_2 powders with their mean crystallite size (from mass% distribution) and the defect concentration (calculated from lattice parameter measurements). If the four TiS_2 powders that exhibit a stoichiometry of $Ti_{1.003}S_2$ are compared, the solid state synthesized powders show the lowest value for cathode utilization. The trend observed in cathode utilizations of these powders agrees well with the trend seen in their crystallite sizes. The differences of 2 to 4% that have been observed in the cathode utilizations of the thio-sol–gel synthesized powders are significant and are not due to errors in measurement. The large crystallite sizes that have been observed in the case of TiS_2 synthesized by the reaction between the elements is clearly detrimental to the electrochemical performance of the powder. The differences in crystallite sizes of the other three powders (reaction A—slow, reaction B—slow and reaction A in acetonitrile—slow) lead to small differences in the corresponding utilization values. Therefore, from these results, it is apparent that although small crystallites are desirable, the increase in utilization diminishes with a corresponding decrease in crystallite size. The effect of crystallite size would, however, be a much more dominant factor in determining the critical current density of these materials.

Similarly, the stoichiometry of TiS_2 also significantly affects the cathode performance. This effect is convincingly illustrated by the performance of the powders obtained from reaction B. The powders obtained from reaction B using fast and slow heat treatment conditions both exhibit the same mean crystallite size, yet there is a significant improvement in utilization (25%) when TiS_2 closer to stoichiometry is achieved using slow cooling rates.

The low temperature precipitation techniques reported by Bensalem and Schleich[12] and by Chianelli and Dines[13] both yield poorly crystalline TiS_2. In Chianelli's method, a precipitate is formed by the reaction of $TiCl_4$ with Li_2S leaving LiCl as an impurity in the sulfide which cannot be completely removed despite repeated washing with tetrahydrofuran. The poor crystalline quality of the powder obtained by reacting $TiCl_4$ with NH_4SH[13] could be improved by heating it in a quartz ampoule at 400 °C along a temperature gradient to allow any NH_4Cl impurities to condense at the cold end. The

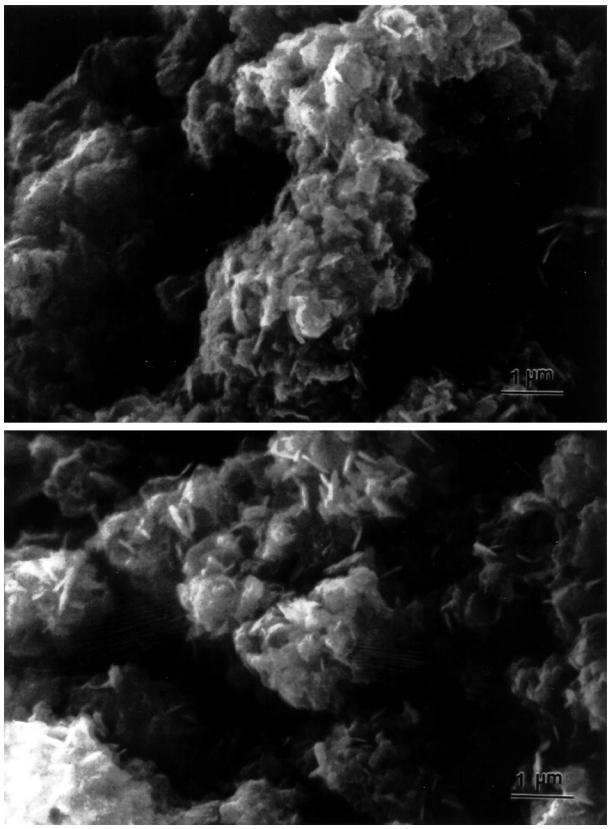

Fig. 7 SEM micrographs of powders obtained from reaction A conducted in acetonitrile heat treated using slow ramping and cooling rates. The crystallite size ranges from less than 0.2 μm to about 0.5 μm.

Table 3 Stoichiometries x in $Ti_{1+x}S_2$ determined by lattice parameter measurements

Process	x in $Ti_{1+x}S_2$
Solid state reaction	0.003
Reaction A (fast)	0.03
Reaction B (fast)	0.03
Reaction A (slow)	0.003
Reaction B (slow)	0.003

defect structure and crystallite sizes of the sulfide obtained by this method have not been reported, however it is possible that an off-stoichiometric sulfide could form since the powders are heated at a higher temperature under vacuum.

The method developed by Bensalem and Schleich[12] can eliminate the problem of contamination due to entrapment of inorganic salts obtained as by-products, although crystalline TiS_2 can be obtained only by heating the powder at a higher temperature. If the precipitate itself has excess titanium, a heat treatment in H_2S at least up to 650 °C would be necessary to revert the stoichiometry back to $x \approx 0$ (in $Ti_{1+x}S_2$), in which case the growth of crystallites would be inevitable. Even if the precipitate has a stoichiometric composition, local defect structures could significantly reduce the performance of the material in batteries. Such behavior has been observed by Kikkawa *et al.*,[14] who have synthesized nearly stoichiometric TiS_2 thin films which are poorly crystalline. These films show a high capacity for the first discharge but the cyclability is poor. They have also postulated that this could be attributed to a local defect structure which resembles the trigonal prismatic coordination seen in TiS_3. Therefore, in the direct precipitation processes, there is little control that can be exercised simultaneously on the defect structure and morphology of the precipitates.

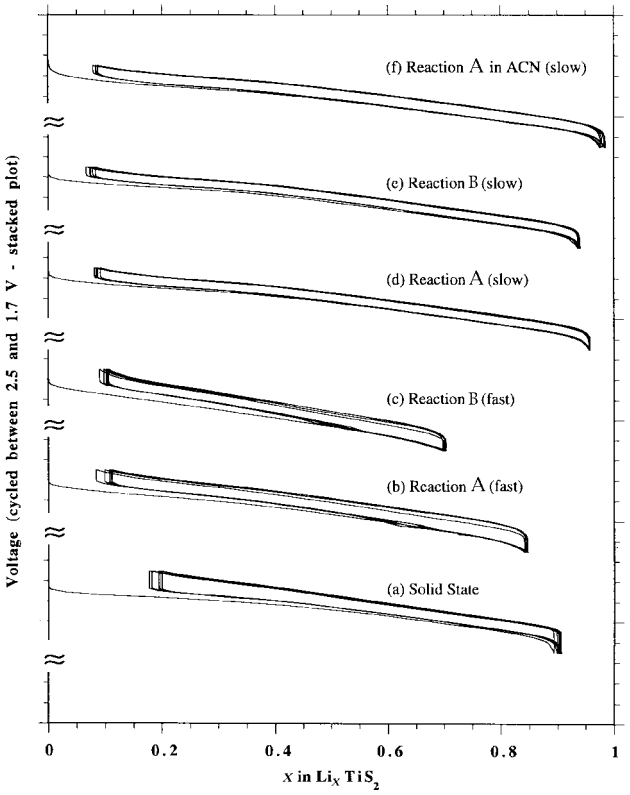

Fig. 8 A comparison of the charge–discharge characteristics of TiS_2 powders synthesized by (a) solid state method, (b) reaction A in benzene + fast heat treatment conditions, (c) reaction B in benzene + fast heat treatment conditions, (d) reaction A in benzene + slow heat treatment conditions, (e) reaction B in benzene + slow heat treatment conditions and (f) reaction A in acetonitrile + slow heat treatment conditions. The cathodes have been cycled between 2.5 and 1.7 V and the plots are shown stacked one above the other. Each plot shows the change in the lithium content when the cathode is cycled between 2.5 and 1.7 V.

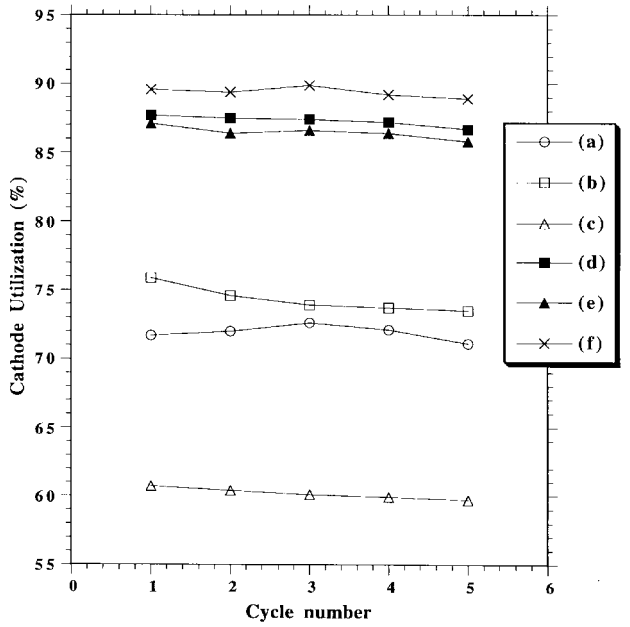

Fig. 9 A comparison of the cathode utilization of TiS_2 powders synthesized by (a) solid state method, (b) reaction A in benzene + fast heat treatment conditions, (c) reaction B in benzene + fast heat treatment conditions, (d) reaction A in benzene + slow heat treatment conditions, (e) reaction B in benzene + slow heat treatment conditions and (f) reaction A in acetonitrile + slow heat treatment conditions.

Table 4 Comparison of platelet size, defect concentration and cathode utilization of TiS_2 powders synthesized using various approaches

Process	Mean size (mass distribution)/μm	x in $Ti_{1+x}S_2$	Cathode utilization (%)[a]
Solid state reaction	3.8	0.003	70±1
Reaction A (fast)	0.6	0.03	73±1
Reaction B (fast)	1.7	0.03	60±1
Reaction A (slow)	0.3	0.003	87±1
Reaction B (slow)	1.7	0.003	85±1
Reaction A in ACN (slow)	—	0.003[b]	89±1

[a]Average calculated from 10 to 15 values. The first discharge cycle has not been included. [b]This value has been estimated, from the observation (and calculations) that identical cooling rates yield sulfides with the same stoichiometry.

4 Summary and conclusions

The thio-sol–gel process offers considerable flexibility in attaining fine particles of TiS_2 with a low interstitial Ti concentration, both of which are essential for obtaining good performance in batteries. The formation of a precursor, although amorphous and deficient in sulfur, introduces the possibility of controlling the defect structure and crystallite size of the sulfide powder. The structure of the precursor can be altered, for example by modifying the alkoxide, changing the solvent system or even by using a different alkoxide. All these factors influence the morphology of the sulfide formed upon heat treatment. Furthermore, the heat treatment conditions can be controlled to affect both the morphology and stoichiometry of the sulfide. The heating rate can change the morphology of the powders, while the cooling rate can be effectively controlled to yield highly stoichiometric TiS_2. A combination of slow and fast heating and cooling rates can be used to vary the crystallite size from 2 to <0.5 μm and the defect concentration (x in $Ti_{1+x}S_2$) in the range $0.03 \leqslant x \leqslant 0.003$. The particle size and the stoichiometry both strongly affect the cathode performance of TiS_2. Thus, careful selection of the reaction conditions in solution and the heat treatment conditions can result in nearly stoichiometric sulfide powders ($x \approx 0.003$ in $Ti_{1+x}S_2$) with fine crystallite sizes ($\leqslant 0.5$ μm). These optimized powders exhibit cathode utilization values as high as 90%, suggesting the overall potential of the thio-sol–gel process.

This work has been possible through the support of the US National Science Foundation Grants DMR 9301014 and a Research Initiation Award (RIA) CTS 9309073, and CTS 9700343. The authors would also like to acknowledge the technical support of Dr. George E. Blomgren of Eveready Battery Co.

Appendix

During cooling, the species that exist in contact with each other are TiS_2, H_2S, H_2, S_2 (assumed as the only dominant S species; in the following calculation this assumption will be justified). The variables in the system are $p(S_2)$, $p(H_2)$, $p(H_2S)$, $[Ti_i^{z+}]$ and temperature (total pressure is constant). There are two independent reactions in the system,

$$TiS_2 \leftrightarrow Ti_i^{z+} + S_2\ (g) + ze^- \quad (5)$$

$$H_2S\ (g) \leftrightarrow H_2\ (g) + 1/2\ S_2\ (g) \quad (6)$$

and two phases, solid and gas. This leaves one degree of freedom. Therefore in the experiments conducted in this work, equilibration at a particular temperature controls the stoichiometry of the material.

The partial pressure of sulfur gas $[p(S_2)]$ was calculated from the decomposition reaction of H_2S at 500, 600, 700 and 800 °C using the standard change in Gibbs energy of the reaction: $\Delta G^\circ = 90290 - 49.39T$ J mol^{-1}.[15] Using the equilibrium partial pressure values, the stoichiometry values were identified from the data compiled by Molenda *et al.*[11] for temperatures of 600, 700 and 800 °C. At the low temperature of 500 °C, the data of Winn and Steele[10] were used to estimate the stoichiometry value. The results of the calculation are plotted in Fig. 10 [as $-\log_{10}(x)$ *vs.* $1/T$] along with a table showing the calculated values of $p(S_2)$ and the value of x in $Ti_{1+x}S_2$. It is clear that as the temperature increases, the decomposition of H_2S proceeds to a larger extent, being an endothermic reaction. However, the stoichiometry is a strong function of temperature and as can be seen from the calculation, at lower temperatures, material closer to stoichiometry can be obtained under equilibrium conditions. A slower cooling rate in an H_2S atmosphere should therefore yield a sulfide closer to stoichiometry, as the sulfide can equilibrate under the conditions prevalent at a lower temperature. This however cannot be continued to much lower temperatures since below approximately 600 °C, the decomposition of H_2S is kinetically limited. Thus significant extrapolation would be necessary to extrude information from the data compiled by Molenda *et al.* at 500 °C. The $p(S_2)$ values calculated are of the order of 10^2 to 10^3 and from a zeroth order approximation, 90 to 95% of this pressure is due to S_2 species (Winn and Steele[10]). The actual equilibrium stoichiometries would be higher by about 0.001 to 0.002. However, the trend of stoichiometry as a function of temperature would still remain the same. The central point (as mentioned above) is the strong dependence of stoichiometry on temperature in comparison to the dependence of $p(S_2)$ on temperature. It should be remembered that the objective of the present study was to identify a trend in the variation of composition with temperature. Hence the calculation of partial pressure of sulfur is based on the assumption that sulfur has reached its equilibrium partial pressure for a given temperature at a total pressure of 1 atmosphere. This may not be the actual case in the present experiment. Nevertheless, the calculation shows the trend and influence of cooling rate on the stoichiometry which is the objective of the present study.

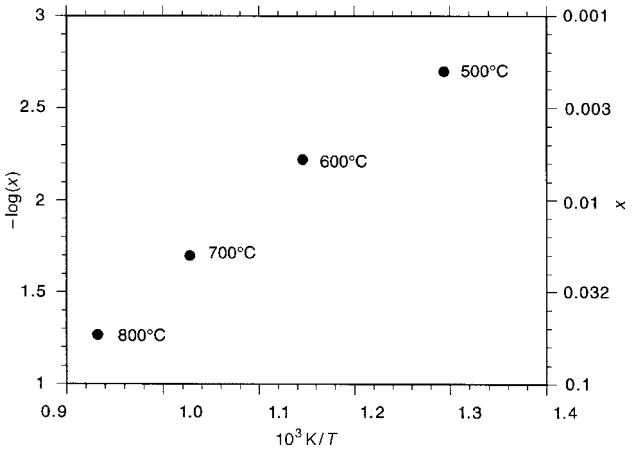

T/°C	$p(S_2)$/Pa	x in $Ti_{1+x}S_2$
500	2.822×10^2	0.002
600	8.13×10^2	0.006
700	1.88×10^3	0.02
800	3.6×10^3	0.054

Fig. 10 A plot of the stoichiometry of TiS_2 (*i.e.* x in $Ti_{1+x}S_2$) as a function of temperature in an H_2S atmosphere assuming equilibrium conditions.

Notes and references

1 A. H. Thompson, F. R. Gamble and C. R. Symon, *Mater. Res. Bull.*, 1975, **10**, 915.

2 M. S. Whittingham, *J. Electrochem. Soc.*, 1976, **123**, 316.
3 M. A. Sriram and P. N. Kumta, *Ceramic Trans.*, 1996, **65**, 163; *Role of Ceramics in Advanced Electrochemical Systems*, ed. P. N. Kumta, G. S. Rohrer and U. Balachandran, American Ceramic Society, Westerville, OH, 1996.
4 K. Kanehori, F. Kirino, Y. Ito, K. Miyauchi and T. Kudo, *J. Electrochem. Soc.*, 1989, **136**, 1265.
5 V. Buck, *Thin Solid Films*, 1986, **139**, 157.
6 P. D. Fleischauer, *Thin Solid Films*, 1987, **154**, 309.
7 R. R. Chianelli, J. C. Scanlon and A. H. Thompson, *Mater. Res. Bull.*, 1975, **10**, 1379.
8 K. Kanehori, F. Kirino, T. Kudo and K. Miyauchi, *J. Electrochem. Soc.*, 1991, **138**, 2216.
9 V. W. Biltz and P. Ehrlich, *Z. Anorg. Allg. Chem.*, 1937, **234**, 97.
10 D. A. Winn and B. C. H. Steele, *Mater. Res. Bull.*, 1976, **11**, 551.
11 J. Molenda, A. Stoklosa, S. Mrowec and D. Than, *Phys. Status Solidi (A)*, 1990, **119**, 571.
12 A. Bensalem and D. M. Schleich, *Mater. Res. Bull.*, 1988, **23**, 857.
13 R. R. Chianelli and M. B. Dines, *Inorg. Chem.*, 1978, **17**, 2758.
14 S. Kikkawa, M. Miyazaki and M. Koizumi, *J. Mater. Res.*, 1990, **5**, 2894.
15 D. R. Gaskell, *Introduction to Metallurgical Thermodynamics*, 2nd edn., McGraw Hill, New York, 1981, p. 586.

Paper 8/02568A